The Caspase-3 homolog DrICE regulates endocytic trafficking during *Drosophila* tracheal morphogenesis

Saoirse S. McSharry[1] and Greg J. Beitel[1*]

Key words: caspase; non-apoptotic; endocytic trafficking; morphogenesis; epithelial tube; *Drosophila*; trachea

[1]Department of Molecular Biosciences, Northwestern University, Evanston, IL 60208, USA

Running title: Caspase-mediated regulation of endocytic trafficking

* Author for correspondence and lead contact: Greg J. Beitel, Hogan Hall, Rm. 2-100, Northwestern University, Evanston, IL 60208, U.S.A., beitel@northwestern.edu, Ph: (847) 467-7776, FAX: (847) 467-1380

ABSTRACT

Although well known for its role in apoptosis, the executioner caspase DrICE has a non-apoptotic function that is required for elongation of the epithelial tubes of the *Drosophila* tracheal system. Here, we show that DrICE acts downstream of the Hippo Network to regulate endocytic trafficking of at least four cell polarity, cell junction and apical extracellular matrix proteins involved in tracheal tube size control: Crumbs, Uninflatable, Kune-Kune and Serpentine. We further show that tracheal cells are competent to undergo apoptosis, even though developmentally-regulated DrICE function rarely kills tracheal cells. Our results reveal a novel developmental role for caspases, a previously unidentified pool of DrICE that colocalizes with Clathrin, and a mechanism by which the Hippo Network controls endocytic trafficking. Given published reports of *in vitro* regulation of endocytosis by mammalian caspases during apoptosis, we propose that caspase-mediated regulation of endocytic trafficking is an evolutionarily conserved function of caspases that can be deployed during morphogenesis.

Epithelial tubes of precise sizes are essential for gas exchange and nutrient delivery in animal tissues. Failure of correct tube sizing can lead to fatal disease[1, 2], yet the cellular and molecular mechanisms that regulate tube size remain poorly understood. To uncover these mechanisms, we study the tracheal system of the *Drosophila* embryo, a ramifying tubular network that serves as the fly's combined pulmonary and vascular systems[3].

The diameter of the largest tube in the tracheal system, the dorsal trunk (DT), increases two-fold as length increases ~15% over a 2.5 h period during mid-embryogenesis, and it does so with no accompanying changes in cell number[4]. Instead, DT dimensions are regulated by a complex set of interacting pathways that all rely on the endocytic system. An apical/lumenal extracellular matrix (aECM) that restricts elongation depends on regulated secretion and endocytosis of matrix-modifying proteins such as Serpentine (Serp)[5]. Basolateral cell-junctional complexes called Septate Junctions (SJs) also restrict DT dimensions. SJs contain a diverse range of proteins including the claudin-family member Kune-Kune (Kune), the FERM-domain protein Yurt (Yrt)[6, 7] and the MAGUK Discs Large (Dlg)[8]. As with the aECM, formation and maintenance of SJs require endocytic trafficking[9]. Apically-localized regulators of DT dimensions also interact with the endocytic pathway, including the polarity protein Crumbs (Crb)[7, 10-13] and the transmembrane protein Uninflatable (Uif)[14]. The endocytic system therefore plays a central role in regulating diverse tracheal size determinants, but how the endocytic pathway is itself regulated in this context is poorly understood.

One candidate pathway that could regulate intracellular trafficking is the highly conserved Hippo Network (HN), which controls growth in diverse organisms and tissues[15]. Organ growth is promoted upon nuclear translocation of the HN effector Yorkie (Yki) in *Drosophila*, or its mammalian homolog Yes-Associated Protein (YAP). Yki and YAP are transcription factors that

activate genes required for growth and resistance to apoptosis, including the Inhibitors of Apoptosis (IAPs), which inactivate caspases[16]. When Yki/YAP activity is low, organ size is typically reduced due to apoptosis resulting from derepressed caspase activity[17]. However, we previously observed that loss of Yki or Death-associated inhibitor of Apoptosis (Diap1*)* causes overelongated trachea despite a normal number of cells. Thus, Yki and Diap1 regulate tube size independently of apoptosis[18].

Here, we show that the caspase-3 homolog DrICE acts downstream of Yki and Diap1 to regulate tracheal elongation. Instead of causing cell death, DrICE regulates endocytic trafficking of tracheal size determinants. This work reveals a novel intersection of the HN, caspases and the endocytic system that has critical functions during normal development. Consistent with previous evidence that mammalian caspases can control endocytic trafficking during apoptosis[19], we propose a model in which regulation of endocytic trafficking is an evolutionarily conserved function of caspases that can be activated with or without triggering cell death, to contribute to morphogenesis or apoptosis, depending on cellular context.

RESULTS

DrICE is necessary and sufficient for tracheal elongation downstream of the Hippo Network

We previously showed that DrICE is required for tracheal dorsal trunk elongation, potentially downstream of the HN[18]. Tracheae fail to elongate normally in embryos homozygous for the *DrICE$^{\Delta 1}$* allele, which deletes the DrICE coding sequence[21], but embryos mutant for Yki and Diap1, both of which negatively regulate DrICE, have overly elongated tracheae at stage 16. These results were consistent with, but did not show, that DrICE acts downstream of Yki and Diap1 in tracheal elongation.

We tested whether reduction of DrICE could suppress the long tracheal phenotypes caused by mutations in Yki, or its transcriptional target Diap1, which is encoded by the *thread (th)* locus[18, 22]. Single loss-of-function mutants *yki*^{B5} and *th*^{J5C8} mutants each have elongated trachea that follow irregular sinusoidal paths (Fig. 1b,f,n), but double mutant trachea of the genotypes *yki*^{B5}; *DrICE*^{17} or *th*^{J5C8}, *DrICE*^{17} are straight and have either WT lengths or have reduced lengths of *DrICE*^{17} mutants (Fig. 1d,e,n). These results indicate that DrICE acts downstream of, or in parallel to, Yki, Diap1 and the HN.

For the above experiments, and most of the subsequent experiments in this report, we used the *DrICE*^{17} allele, which has a point mutation[23] in a region near the substrate binding site of DrICE. However, in contrast to a previous report that *DrICE*^{17} is a protein-null allele[23], using different antibodies we find that *DrICE*^{17} generates a stable protein (Fig. 1o and Fig. 2e-f), and causes a stronger tracheal phenotype than *DrICE*$^{\Delta 1}$, the null allele[18]. Thus, *DrICE*^{17} behaves as a dominant negative allele that competes with maternally contributed DrICE.

To distinguish between DrICE acting “downstream of” and “in parallel to” the HN in tracheal development, we used western blotting on stage 16 embryos to show that wild-type (WT) DrICE protein levels are elevated by approximately 50% in both *yki*^{B5} and *th*^{J5C8} mutant embryos (Fig. 1o). Together, these results confirm that DrICE is necessary for dorsal trunk elongation and that DrICE acts downstream of the HN.

We then asked if DrICE expression is sufficient to drive tracheal elongation without increased upstream HN activity by expressing UAS-DrICE in the tracheal system using the *breathless (btl)-Gal4* driver[24, 25]. This overexpression results in elongated tracheae, similar to *yki*^{B5} mutants (Fig. 1c,n and 2i-j’’’). DrICE is therefore necessary and sufficient to drive tracheal elongation.

Tracheal cells are not refractory to apoptosis

Although the executioner caspase DrICE is necessary for tracheal elongation, few (<3%) tracheal cells undergo apoptosis during wild-type morphogenesis.[26] This raises the question of how a caspase can act in a developmental process without triggering apoptosis. We investigated the possibility that apoptosis maybe disabled in the developing trachea by analyzing loss-of-function mutants for the caspase inhibitor Diap1 (th^{J5C8}). We previously showed that th^{J5C8} mutant embryos with contiguous dorsal trunks have elongated trachea despite a WT number of cells[18], but a more comprehensive analysis of th^{J5C8} mutants here revealed that the majority of th^{J5C8} embryos, are in fact missing dorsal trunk segments (Fig. 1i). Strikingly, 25% of heterozygous th^{J5C8} embryos displayed missing tracheal segments (Fig. 1l), suggesting that tracheal cells are capable of undergoing caspase-mediated apoptosis.

We confirmed the existence of apoptosis in *th* mutant trachea by counting the number of tracheal nuclei. In stage 16 th^{J5C8} DT segments, tracheal cell number is reduced by an average of 55% compared to WT ($p<0.0001$ for DT segments 5-6, Fig. 1m). Notably, average DT cell number drops from 26 in WT to 15 in *th* DT segments that are intact, and to only 10 in broken DTs, suggesting that there is a minimal number of cells that are required to assemble or maintain DT segments (Fig. 1m). Further evidence that the missing tracheal cells in *th* mutants underwent caspase-mediated apoptosis is provided by the presence of cells with strong cleaved caspase staining in *th* mutants (Fig. S2a), and by the 150% suppression of DT breaks and 140% increase in the number of tracheal cells in th^{J5C8} $DrICE^{17}$ mutants (Fig. 1m). Thus, the apoptotic roles of Diap1 and DrICE are maintained in tracheal cells during normal morphogenesis.

Interestingly, in contrast to th^{J5C8} mutants, loss of Yki, which is a key transcriptional co-activator of Diap1[27, 28], does not induce DT breaks and only reduces tracheal cell number from 26 to 21 (Fig. 1m). This observation suggests that a basal level of Diap1 expression may protect tracheal

cells from DrICE-mediated apoptosis in *yki*^{B5} mutants, yet still allow elevated DrICE activity to elongate tracheal cells.

To further test the apoptotic potential of tracheal cells, we expressed the pro-apoptotic genes Grim and Reaper [29] in the developing trachea using the *btl*:*Gal4* tracheal driver. Overexpression of Grim largely eliminates the tracheal system (Fig. 1g). Reaper overexpression results in the loss of one or two tracheal dorsal trunk segments in most embryos, similar to the homozygous *th*^{J5C8} mutant phenotype (Fig. 1h,i). Critically, the lethal effects of Grim overexpression are dominantly suppressed by one copy of the *DrICE*^{17} allele (Fig. 1j), and homozygous *DrICE*^{17} blocks the ability of Grim to destroy the tracheal system (Fig. 1k). Taken together, these results demonstrate that tracheal cells are not refractory to apoptosis— they have a functional caspase-dependent apoptotic system that does not kill cells during normal development, despite the requirement for DrICE in tracheal elongation.

A pool of DrICE localizes to punctae enriched at the tracheal apical surface

To explore the mechanism by which DrICE mediates tracheal elongation, we considered whether DrICE might be spatially compartmentalized in non-apoptotic cells, as is the case for the initiator caspase Dronc, which Amcheslavsky *et al.* showed was localized basally for non-apoptotic roles in larval imaginal discs[30]. Staining with the α–DrICE^{SK31} antibody, raised against full-length DrICE protein[31, 32], produces a diffuse cytoplasmic signal in WT trachea that is greatly reduced in the nucleus (Fig. 2a). A different pattern of staining is observed with the α–DrICE^{CST9478} antibody, which is raised against a peptide N-terminal to the Asp230 cleavage site of DrICE and is reported to preferentially recognize the cleaved form of DrICE (Cell Signaling Technologies, #9478). α–DrICE^{CST9478} signal is localized to numerous cytosolic punctae that are enriched at the apical surface of tracheal cells, particularly during stages 13 and 14 (Fig. 2b, Fig. S1b,e,h,k). Thus, there

is a pool of DrICE that is localized separately from the inhibitor Diap1 which could potentially allow DrICE to elongate the trachea without triggering apoptosis.

DrICE partially co-localizes with Clathrin

The punctate pattern of α–DrICE^{CST9478} signal resembles that of intracellular trafficking machinery, suggesting that this pool of DrICE may associate with trafficking compartments. We tested for colocalization of α–DrICE^{CST9478} signal with markers of endocytic vesicle formation (Clathrin), and for early (Rab5), recycling (Rab11), or late (Rab7) endosomes. Punctate DrICE^{CST9478} signal partially overlaps with Clathrin both at the apical surface and in cytosolic regions (yellow arrowheads, yellow box and inset in Fig. 2l-l", respectively; 23% overlap; Pearson R= 0.25). However, there is only sporadic co-localization with Rab5 (Fig. 2m-m"; 3.8% overlap, R=0.06), Rab11 (Fig. 2n-n"; 6% overlap, R=0.1) or Rab7 (2% overlap, R=0.12, Fig. 2o-o'') early, late and recycling endosomes respectively. The pool of DrICE defined by α–DrICE^{CST9478} is therefore positioned to regulate tracheal size by influencing Clathrin-mediated endocytosis and subsequent trafficking of proteins that determine tracheal size. In addition, the incomplete co-localization of DrICE^{CST9478} signal with Clathrin suggests that multiple pools of DrICE exist, which supports the idea that DrICE acts in multiple independent functions, including apoptosis.

In addition to its role in early endocytosis, Clathrin also mediates protein trafficking from the transgolgi network (TGN). Because the overlap of Clathrin with DrICE appears to be both apical and cytosolic (Fig. 2 l-l", arrowheads), the intracellular co-localization of α–DrICE^{CST9478} signal and Clathrin suggests that DrICE could also influence Clathrin-mediated TGN trafficking.

DrICE co-localizes with and alters the intracellular trafficking and/or levels of apical tracheal size determinants

Because transmembrane determinants of tracheal tube size including Crb and Uif are known to be trafficked through endocytic compartments[10, 11], we asked if DrICE associates with compartments containing these proteins. In WT stage 16 tracheae, DrICE^{CST9478} signal partially overlaps with Uif (Fig. 2b-b", 12% colocalization, Pearson correlation R=0.21; Fig. S1b",e",h",k") and Crb (Fig. S1k'', 17% colocalization, R=0.27), but shows stronger overlap with Crb at the apical surface during tube expansion at stages 13-14 (Supplementary Fig. 1b'',e''). An apical pool of DrICE is therefore positioned to directly regulate trafficking of apical markers.

We tested if there were functional interactions between DrICE and transmembrane apical markers by examining Crb and Uif in *DrICE^{17}* mutants. Overall apical/basal polarity as assessed by Crb staining is largely unaffected in *DrICE^{17}* mutations. Levels of apical and cytosolic Crb are not significantly altered in *DrICE^{17}* mutants at stage 16, but in stage 14 embryos, fewer Crb-positive cytosolic punctae were visible in *DrICE^{17}* mutants than in WT ($p<0.05$, Fig.3a-b, j) and conversely more punctae were present in *yki^{B5}* mutant trachea than in WT ($p<0.005$, Fig. 3a, c, j). Similarly, over-expression of DrICE in the tracheal system increases Crb levels at stage 16 ($p<0.0005$, Fig. 3m,n). No significant changes in Uif abundance or distribution were observed in *DrICE* mutant tracheae (Fig. 2f,f",h,h"), but *DrICE^{17}* suppresses the increased abundance of Uif positive punctae in the tracheae of embryos mutant for the basolateral polarity protein Yurt ($p<0.005$; Fig. 4a-e). Moreover, *DrICE^{17}* also suppresses the increased tracheal length of the *yrt^{65A}* mutants ($p<0.005$, Fig. 4f).

DrICE alters the trafficking of tracheal junctional components

We tested whether DrICE mutants exhibited alterations in trafficking of basolateral junctional components, which are known to be constitutively recycled through the endocytic system through

tracheal development [33, 34]. Immunostaining for the claudin Kune-Kune (Kune) revealed that junctional and overall levels of Kune are reduced in *yki*^{B5} trachea ($p<0.05$; Fig. 3e, k), and in trachea overexpressing DrICE (Fig. 3m'), both conditions in which DrICE is elevated. Conversely, in *DrICE*^{17} mutants, strong ectopic staining for Kune is apparent at the apical (lumenal) surface and overall levels of Kune are increased (Fig. 3f, k). However, not all SJ components are negatively regulated by *DrICE*. For example, levels of the MAGUK Discs Large (Dlg) were only modestly affected in *yki*^{B5} and *DrICE*^{17} mutants (Fig. 3g-i), and we previously reported that the FERM-domain protein Coracle was unaffected by Yki and DrICE mutations. Thus, DrICE does not globally regulate endocytic trafficking, but rather is required for trafficking of a subset of tracheal markers.

DrICE colocalizes with and alters the trafficking of lumenal tracheal determinant Serpentine

We investigated whether DrICE is required for trafficking of lumenal determinants required for tracheal size control, including the putative chitin deacetylase Serpentine (Serp). As with the apical determinant Uif, we found that *DrICE*^{17} suppresses the overabundance of Serp-containing punctae in *yrt*^{65A} ($p<0.05$; Fig. 4a'-e). Furthermore, overactivation of DrICE resulting from loss of *yki* decreases the amount of lumenal Serp in tracheal anterior, a phenotype that is partially suppressed by *DrICE*^{17} ($p<0.005$; green in Fig. 4g-k"). DrICE therefore affects trafficking of lumenal tracheal size determinants and mediates the effects of the HN on their trafficking.

Together, these results reveal that DrICE activity selectively modulates the trafficking of cargo originating from both the apical and basolateral membranes, and at minimum affects the trafficking of at least four different proteins required for tracheal size control.

DISCUSSION

Our work shows for the first time that a caspase regulates endocytic trafficking during normal morphogenesis. Moreover, the caspase activity responsible for the endocytic function does not trigger apoptosis, even though the cells are competent to undergo caspase-mediated apoptosis. We also demonstrate a previously unidentified link between the Hippo Network (HN) and the endocytic system. While previous studies focused on the effects of the endocytic system on the *output* of the Hippo Network[35-38], we report the converse: the Hippo Network acts as *input* to the endocytic system that alters endocytic trafficking.

A notable aspect of the role of DrICE in trafficking is that DrICE is required for trafficking of select—not all—trafficked cargo. For example, the abundance and localization of the SJ protein Kune is affected by alterations in DrICE, but Coracle and Dlg are not strongly affected (Fig. 3i,j and [18]). We also observe defects in the trafficking of the lumenal protein Serp, but no defects have been observed in the trafficking of the similar chitin deacetylase Vermiform (Verm)[18]. The differential trafficking of Serp and Verm in DrICE mutants is commensurate with observations by Dong et. al[11], who observed that a mutation in *shrub/VPS32* that disrupts multivesicular body formation also altered the localization of Serp, but not Verm. This similar differential effect on Verm and Serp trafficking provides further evidence of the involvement of DrICE in endocytosis. It is also notable that not only does DrICE regulate specific cargos, the effect on each cargo is also cargo specific. For example, DrICE activity *promotes* Crb accumulation, but *suppresses* Kune accumulation. These results are consistent with DrICE acting directly of individual cargos, or on cargo-adapters such as sorting adapters, or on both cargo and adapters.

The counterintuitive requirement of an executioner caspase to promote growth in an epithelium has not previously been reported in mammals. However, there is *in vitro* evidence that mammalian caspases regulate endocytic trafficking[20]. For example, Duclos et al. showed that activation of

activator and effector caspases in HeLa and HEK293 cells resulted in cleavage of Sorting Nexins 1 and 2 (SNX1 and SNX2), which control intracellular trafficking of specific cargos[19]. Cleaved SNX increased activation of the hepatocyte growth factor receptor (HGFR) and ERK1/2 signaling. Additionally, Han et al. showed that caspase-3 cleavage of junctional component Gap43 was required for endocytosis of the AMPA receptor A in non-apoptotic cells in vitro[39]. Together, the previously published *in vitro* mammalian results and these *in vivo Drosophila* results suggest a new developmental role for caspase-mediated regulation of endocytic trafficking that is evolutionarily conserved and may also function in mammalian development.

The conserved involvement of caspases in endocytic trafficking raises the possibility that there is a deeper mechanistic connection between apoptosis and trafficking of junctional components. In the current model of apoptosis, caspase-mediated proteolysis of cell junctions results in decreased cell adhesion, which allows an apoptotic cell to be cleanly extruded from an epithelium (Fig. 5, middle; reviewed by [40]). However, in mammals and flies, junctional components are constitutively cycled through the endocytic system even in non-apoptotic epithelia[33, 34, 41]. This presents an opportunity for caspases to alter trafficking of junctional components. Perhaps the ability of caspases to regulate endocytic trafficking arose as an ancient apoptotic function that allowed dying epithelial cells to more efficiently downregulate junctions by using both endocytosis and caspase-mediated proteolysis rather than caspase-mediated proteolysis alone (Fig. 5, bottom). We hypothesize that caspase-mediated alterations in cell junction trafficking has been co-opted in morphogenesis, when growing epithelia require rapid remodeling of junctional components (Fig. 5, top).

Experimental evidence from mammalian cerebral ischemic injury supports the proposed model that limited activation of caspases alters junctional endocytosis. During cerebral ischemic injury, blood flow in the brain is blocked, which leads to extensive caspase activation, downregulation of

claudin-based tight junctions, and a large and damaging increase in vascular permeability[42]. Pretreatment of tissue with caspase inhibitors increases junctional continuity and integrity including junction components claudin-5 and the tight junction marker ZO-1, and ultimately reduces tissue damage. Strikingly, more endothelial cells show caspase activation than undergo apoptosis, suggesting that caspase activation is sufficient to induce junctional downregulation and vascular permeability.

The ability of caspases to regulate endocytic trafficking has significant implications for cancer treatments, which frequently result in caspase activation. Sub-apoptotic activation of effector caspases in surviving tumor cells after anti-cancer treatment could potentially result in reduced junctional integrity, which could further promote epithelial-to-mesenchymal transformation (EMT) and metastasis. Additionally, caspase-driven changes in the trafficking of polarity proteins such as Crb and of growth factor receptors could also contribute to EMT and disease progression. Consistent with this possibility, previous evidence has indicated that human Caspase-3 is required for migration, invasion and metastasis HCT116 colon cancer cells[43], and for tumor cell repopulation upon irradiation[44].

In summary, this work reveals a novel function of the effector caspase DrICE during development: modulating endocytic trafficking of cell junctional components and signaling molecules. Given that mammalian effector caspases can also modulate endocytic trafficking, we propose that regulation of the trafficking of junctional components is a conserved caspase function that can be brought into play during normal morphogenesis or in pathologic conditions by localized, sub-apoptotic caspase activation.

FIGURE LEGENDS

Fig. 1: The executioner caspase DrICE acts downstream of the Hippo Network to elongate tracheal tubes during development without triggering apoptosis.

(a-l) Compared to WT (w^{1118}, stage 16) (a), the dorsal trunks (DTs) of yki^{B5} mutant embryos and embryos expressing full-length DrICE in the tracheal system (*btl>DrICE*) are elongated (b,c), while DTs in $drICE^{17}$ are too short (d). $DrICE^{17}$ is epistatic to yki^{B5} since yki^{B5}; $DrICE^{17}$ double mutants do not have long trachea (e). Loss of the DrICE inhibitor Diap1/*th* can cause tracheal over-elongation (f), but also causes missing DT segments when homozygous (i) or heterozygous (l). Tracheal expression of the pro-apoptotic genes *Grim* (g) or *Reaper* (h) causes severe or moderate segment loss, respectively, that is partially or fully suppressed by one or two copies of $DrICE^{17}$ (j, k). Red arrows in g mark remnants of the tracheal system, while yellow arrowheads in h-l mark missing dorsal trunk segments. Scale bar for a-l in a, 25 μm. Source data are provided as a source data file.

(m) Loss of the DrICE inhibitor Diap1 (th^{J5C8}) causes a dramatic decrease in the number of embryos with intact dorsal trunks (*N*=17 embryos over 5 experiments), which can be suppressed by concomitant mutation of DrICE (*N*=20 over 3 experiments). Large decreases in tracheal cell number also occur in the th^{J5C8} mutation, suggesting the broken trunks are due to increased cell death (N=6 embryos total: 3 broken, 3 intact). Consistent with broken trachea as a consequence of apoptosis, the loss of intact trachea and overall cell numbers in th^{J5C8} can both be suppressed by $DrICE^{17}$ (*N*=4). Neither dramatic cell death nor dorsal trunks breaks are present in yki^{B5} embryos (*N*=4). Each data point is represented as a point. Error bars, S.E.M. Source data are provided as a source data file.

(n) Quantification of DT length in single and double mutant combinations of HN and DrICE mutants, and in embryos overexpressing DrICE. DT length normalized to WT (w^{1118}) (*N*=10) for HN and DrICE mutants, and to *btl-Gal4, UAS-GFP/+* for overexpressed DrICE (*btl-Gal4 UAS-*

GFP/+; UAS-DrICE/+) ($N \geq 5$ for all except N=4 for *th*^{J5C8};*DrICE*^{17}). Each data point is represented as a point. Error bars, S.E.M. Source data are provided as a source data file.

(o) Western blot quantification of DrICE protein abundance in stage 16 embryos using the α-DrICE^{CST13085} antibody that recognizes full-length DrICE. A representative blot is shown in Fig. S1i, the 47kDa DrICE full-length band was quantified relative to total protein from at least three experiments. Note that DrICE protein levels in *DrICE*^{17} homozygotes are not different than WT, which is consistent with *DrICE*^{17} being a dominant negative allele that causes more severe tracheal phenotypes than the DrICE$^{\Delta 1}$ null allele[18] (n,o). (N=4 blots).

For all graphs, each data point is indicated as a dot. Error bars, S.E.M. *p<0.05; **, p<0.005; ***, p<0.0005. Source data are provided as a source data file.

Fig. 2: A pool of DrICE partially co-localizes with Clathrin.

(a-j'''') Staining with the α-DrICE^{SK31} antibody against full-length DrICE (a,c,e,g,i) reveals broad cytoplasmic signal in WT trachea (a) that is reduced in trachea zygotically homozygous for the null allele *DrICE*$^{\Delta 1}$ (g) and elevated in trachea overexpressing DrICE (i). Staining with α-DrICE^{CST9478} (b,d,f,h,j), which was raised against a peptide containing the DrICE sequence that is cleaved during activation, reveals a more restricted punctate pattern that is enriched at the tracheal apical surface in WT trachea (dashed blue lines), and particularly at earlier developmental stages (Supplemental Fig. 1b,e). α-DrICE^{CST9478} signal is reduced in *DrICE*$^{\Delta 1}$ trachea (h), elevated in trachea overexpressing DrICE (j). DrICE^{CST9478} signal in h results from the maternal contribution of DrICE that is also observed by western blot in Fig. 1o (representative gel image in Fig. S1l) and is absent in late larval tissue (Fig. S2 d-g).

(k) Partial schematic of the endocytic system showing the roles of endocytic markers.

(l-o") Localization of DrICE^{CST9478} signal with markers of the endocytic system in WT *(w^{1118})* trachea. α-DrICE^{CST9478} signal shows partial colocalization with Clathrin (l) but not and Rab5 (m), with Rab11 (n) or Rab7 (o). Colocalization was quantified in 2 ROIs in each of *N*≥3 z-slices for *N*≥4 embryos. Source data are provided as a source data file.

Blues dashed lines mark the apical cell surface, white dashed lines mark the basal cell surface. Scale bar for a-j" in j", 5 μm; for l-o" in o", 5 μm.

Fig. 3: DrICE is required for normal levels and localization of the tracheal size determinants Crb and Kune in the trachea

(a-c) The number of cytosolic Crb punctae (yellow arrowheads) is increased in *yki^{B5}* mutants (b), but decreased in *DrICE^{17}* mutants (c) compared to WT (w^{1118}) (a) at stage 14.

(d-f) Cytoplasmic Kune abundance is decreased in *yki^{B5}* and increased in *DrICE^{17}* relative to *w^{1118}*. Quantification in k.

(g-i) The levels of the basolateral septate junction protein Dlg appear minimally affected in *yki^{B5}* and *DrICE^{17}* mutants, indicating that the ability of DrICE to regulate trafficking is selective.

(j) Boxplot showing the number of cytoplasmic punctae of Crumbs at embryonic stage 14 is reduced in *DrICE^{17}* tracheal cells compared to *w^{1118}* and increased in *yki^{B5}* relative to *w^{1118}*. Number of punctae was counted in 2 ROIs in each of 2 *z*-slices for *N*≥5 embryos and normalized to ROI area. Center line represents the median, box limits are the upper and lower quartiles, whiskers are 1.5X interquartile range, each data point is represented as a point. Source data are provided as a source data file.

(k) Mean intensity of Kune in a maximum projection of the fifth tracheal metamere was measured in N≥5 embryos of each genotype then normalized to the WT (*w^{1118}*) control. Each data point is represented as a point. Error bars, S.E.M. Source data are provided as a source data file.

(l-m'') Overexpression of DrICE in the trachea increases Crb levels relative to the control at stage 16 (l vs. m), consistent with the decrease of Crb punctae in stage 14 *DrICE*^{17} mutants. Quantified in **m**. Conversely, Kune levels are decreased when DrICE is overexpressed (l' vs. m').

(n) Cytoplasmic Crb abundance is dramatically increased in *btl>DrICE* relative to *btl>Gal4/+*. Mean Kune intensity was measured in 2 ROIs in each of 5 *z*-slices for *N*=4 embryos of each genotype and quantified relative to the *btl>Gal4/+* control. Each data point is represented as a point. Error bars, S.E.M. Source data are provided as a source data file.

Blues dashed lines mark the apical cell surface, white dashed lines mark the basal cell surface. Scale bar for a-i in i, 2.5 μm; for l-m" in m", 2.5 μm. *p<0.05; **, p<0.005; ***, p<0.0005.

Fig. 4: DrICE is required for endocytic trafficking of lumenal tracheal size determinant Serpentine and apical determinant Uif.

(a-e) Mutation of the basolateral polarity protein Yurt (*yrt*^{65A}) causes abnormal intracellular accumulation of the tracheal size determinants Uif (b, arrowhead) and Serp (b', arrowhead), an effect that is suppressed by *DrICE*^{17} (c-c'). White dashed lines outline basal cell surface; blue dashed lines outline apical surface. Scale bar a-d' in d', 5 μm. Relative number of cytoplasmic punctae quantified in (e), where the number of punctae in each of two ROIs in a maximum projection of *yrt*^{65A} (*N*=5 embryos), *yrt*^{65A}/+ (*N*=5 embryos), and *yrt*^{65A}, *DrICE*^{17} (*N*=6 embryos) was counted, then divided by the area of the given ROI. Resulting number of punctae per area is reported relative to *yrt*^{65A}/+.

(f) The *DrICE*^{17} mutation suppresses tracheal overelongation caused by a mutation in the basolateral polarity gene *yrt*. Quantification of tracheal DT length at stage 16 for *yurt*^{65A} (*N*=6) and *yurt*^{65A}, *DrICE*^{17} (*N*=7) and *DrICE*^{17} (*N*=5) mutants reveals that *yurt*^{65A}, *DrICE*^{17} double mutants are shorter than *yurt*^{65A} mutants. Tracheal lengths normalized to body length and reported

relative to WT (w^{1118}). For all graphs, each data point is represented as a point. Error bars, S.E.M. Source data are provided as a source data file.

(g-k") Mutation of the Hippo Network component Yki (yki^{B5}) reduces the levels of Serp (green) in the tracheal anterior relative to the lumenal chitin binding protein Gasp, marked by staining with the monoclonal antibody 2A12 (arrowhead, i). This reduction is suppressed by $DrICE^{17}$ (j). (g) Quantification of the mean intensity of Serp divided by the mean intensity of 2A12 in a maximum projection of *N*=4 embryos for WT (w^{1118}), *N*=4 embryos for yki^{B5}; $DrICE^{17}$, *N*=7 embryos for yki^{B5}, *N*= 3 embryos for $DrICE^{17}$; Numbers reported as relative to w^{1118}. Scale bar h-k"' in k", 12.5 μm. Source data are provided as a source data file.

Fig. 5: Model for caspase-regulated endocytic trafficking in apoptosis

See main text for details.

DATA AVAILABILITY

The authors declare that the main data supporting the findings of this study are available within the article and its Supplementary Information files. Extra data are available from the corresponding author upon request.

ACKNOWLEDGEMENTS

For reagents we thank Rob Ward (α-Uif), Pascal Meier (α- $DrICE^{SK31}$), Christos Samakovlis (α-MTf), Matthias Behr (α-Clathrin). We also thank Benjamin Kraft for assistance in epistasis experiments; Andreas Bergmann for helpful discussions; J. Hornick and the Northwestern University Biological Imaging Facility for technical and imaging support; and Laura Lackner, Heike Fölsch, and I. Tanelli Helenius for comments on the manuscript. Stocks obtained from the Bloomington Drosophila Stock Center (NIH P40OD018537) were used in this study, and

FlyBase was a critical resource [45]. This work was supported by NIH RO1GM108964 to GJB. S. McSharry was supported by the National Institute of General Medical Sciences training grant T32GM008061.

AUTHOR CONTRIBUTIONS

SM and GJB conceived and designed the experiments. SM performed the experiments. SM and GJB analyzed the data. SM and GJB wrote the manuscript.

DECLARATION OF INTERESTS

All authors declare no competing interests.

REFERENCES

1. Cooper, A.D., Campeau, N.G. & Meissner, I. Susceptibility-weighted imaging in familial cerebral cavernous malformations. *Neurology* **71**, 382 (2008).
2. Faguer, S. *et al.* Massively enlarged polycystic kidneys in monozygotic twins with TCF2/HNF-1beta (hepatocyte nuclear factor-1beta) heterozygous whole-gene deletion. *American journal of kidney diseases : the official journal of the National Kidney Foundation* **50**, 1023-1027 (2007).
3. Zuo, L., Iordanou, E., Chandran, R.R. & Jiang, L. Novel mechanisms of tube-size regulation revealed by the Drosophila trachea. *Cell Tissue Res* **354**, 343-354 (2013).
4. Beitel, G.J. & Krasnow, M.A. Genetic control of epithelial tube size in the Drosophila tracheal system. *Development* **127**, 3271-3282 (2000).
5. Tsarouhas, V. *et al.* Sequential pulses of apical epithelial secretion and endocytosis drive airway maturation in Drosophila. *Developmental cell* **13**, 214-225 (2007).
6. Nelson, K.S., Furuse, M. & Beitel, G.J. The Drosophila Claudin Kune-kune is required for septate junction organization and tracheal tube size control. *Genetics* **185**, 831-839 (2010).
7. Laprise, P. *et al.* Epithelial polarity proteins regulate Drosophila tracheal tube size in parallel to the luminal matrix pathway. *Current biology : CB* **20**, 55-61 (2010).
8. Woods, D.F. & Bryant, P.J. The discs-large tumor suppressor gene of Drosophila encodes a guanylate kinase homolog localized at septate junctions. *Cell* **66**, 451-464 (1991).
9. de Vreede, G. *et al.* The Scribble module regulates retromer-dependent endocytic trafficking during epithelial polarization. *Development* **141**, 2796-2802 (2014).
10. Olivares-Castineira, I. & Llimargas, M. EGFR controls Drosophila tracheal tube elongation by intracellular trafficking regulation. *PLoS genetics* **13**, e1006882 (2017).
11. Dong, B., Hannezo, E. & Hayashi, S. Balance between apical membrane growth and luminal matrix resistance determines epithelial tubule shape. *Cell reports* **7**, 941-950 (2014).
12. Tepass, U., Theres, C. & Knust, E. crumbs encodes an EGF-like protein expressed on apical membranes of Drosophila epithelial cells and required for organization of epithelia. *Cell* **61**, 787-799 (1990).
13. Tepass, U. & Knust, E. Phenotypic and developmental analysis of mutations at thecrumbs locus, a gene required for the development of epithelia inDrosophila melanogaster. *Roux Arch Dev Biol* **199**, 189-206 (1990).
14. Zhang, L. & Ward, R.E.t. uninflatable encodes a novel ectodermal apical surface protein required for tracheal inflation in Drosophila. *Developmental biology* **336**, 201-212 (2009).

15. Yu, F.X., Zhao, B. & Guan, K.L. Hippo Pathway in Organ Size Control, Tissue Homeostasis, and Cancer. *Cell* **163**, 811-828 (2015).
16. Salvesen, G.S. & Duckett, C.S. IAP proteins: blocking the road to death's door. *Nature reviews. Molecular cell biology* **3**, 401-410 (2002).
17. Verghese, S., Bedi, S. & Kango-Singh, M. Hippo signalling controls Dronc activity to regulate organ size in Drosophila. *Cell death and differentiation* **19**, 1664-1676 (2012).
18. Robbins, R.M., Gbur, S.C. & Beitel, G.J. Non-canonical roles for Yorkie and Drosophila Inhibitor of Apoptosis 1 in epithelial tube size control. *PloS one* **9**, e101609 (2014).
19. Duclos, C.M. *et al.* Caspase-mediated proteolysis of the sorting nexin 2 disrupts retromer assembly and potentiates Met/hepatocyte growth factor receptor signaling. *Cell Death Discov* **3**, 16100 (2017).
20. Duclos, C., Lavoie, C. & Denault, J.B. Caspases rule the intracellular trafficking cartel. *FEBS J* **284**, 1394-1420 (2017).
21. Muro, I. *et al.* The Drosophila caspase Ice is important for many apoptotic cell deaths and for spermatid individualization, a nonapoptotic process. *Development* **133**, 3305-3315 (2006).
22. Huang, J., Wu, S., Barrera, J., Matthews, K. & Pan, D. The Hippo signaling pathway coordinately regulates cell proliferation and apoptosis by inactivating Yorkie, the Drosophila Homolog of YAP. *Cell* **122**, 421-434 (2005).
23. Xu, D. *et al.* The effector caspases drICE and dcp-1 have partially overlapping functions in the apoptotic pathway in Drosophila. *Cell death and differentiation* **13**, 1697-1706 (2006).
24. Brand, A.H. & Perrimon, N. Targeted gene expression as a means of altering cell fates and generating dominant phenotypes. *Development* **118**, 401-415 (1993).
25. Shiga, Y., TanakaMatakatsu, M. & Hayashi, S. A nuclear GFP beta-galactosidase fusion protein as a marker for morphogenesis in living Drosophila. *Dev Growth Differ* **38**, 99-106 (1996).
26. Baer, M.M. *et al.* The role of apoptosis in shaping the tracheal system in the Drosophila embryo. *Mechanisms of development* **127**, 28-35 (2010).
27. Harvey, K.F., Pfleger, C.M. & Hariharan, I.K. The Drosophila Mst ortholog, hippo, restricts growth and cell proliferation and promotes apoptosis. *Cell* **114**, 457-467 (2003).
28. Tapon, N. *et al.* salvador Promotes both cell cycle exit and apoptosis in Drosophila and is mutated in human cancer cell lines. *Cell* **110**, 467-478 (2002).
29. Goyal, L., McCall, K., Agapite, J., Hartwieg, E. & Steller, H. Induction of apoptosis by Drosophila reaper, hid and grim through inhibition of IAP function. *The EMBO journal* **19**, 589-597 (2000).
30. Amcheslavsky, A. *et al.* Plasma Membrane Localization of Apoptotic Caspases for Non-apoptotic Functions. *Developmental cell* **45**, 450-464 e453 (2018).
31. Ditzel, M. *et al.* Inactivation of effector caspases through nondegradative polyubiquitylation. *Molecular cell* **32**, 540-553 (2008).
32. Zachariou, A. *et al.* IAP-antagonists exhibit non-redundant modes of action through differential DIAP1 binding. *Embo Journal* **22**, 6642-6652 (2003).
33. Tiklova, K., Senti, K.A., Wang, S., Graslund, A. & Samakovlis, C. Epithelial septate junction assembly relies on melanotransferrin iron binding and endocytosis in Drosophila. *Nature cell biology* **12**, 1071-1077 (2010).
34. Peglion, F., Llense, F. & Etienne-Manneville, S. Adherens junction treadmilling during collective migration. *Nature cell biology* **16**, 639-651 (2014).
35. Kwon, Y. *et al.* The Hippo signaling pathway interactome. *Science* **342**, 737-740 (2013).
36. Wang, W. *et al.* Defining the protein-protein interaction network of the human hippo pathway. *Molecular & cellular proteomics : MCP* **13**, 119-131 (2014).
37. Couzens, A.L. *et al.* Protein interaction network of the mammalian Hippo pathway reveals mechanisms of kinase-phosphatase interactions. *Science signaling* **6**, rs15 (2013).
38. Cox, C.M. *et al.* Endosomal regulation of contact inhibition through the AMOT:YAP pathway. *Molecular biology of the cell* **26**, 2673-2684 (2015).
39. Han, M.H. *et al.* The novel caspase-3 substrate Gap43 is involved in AMPA receptor endocytosis and long-term depression. *Molecular & cellular proteomics : MCP* **12**, 3719-3731 (2013).
40. Andrade, D. & Rosenblatt, J. Apoptotic regulation of epithelial cellular extrusion. *Apoptosis* **16**, 491-501 (2011).
41. Green, K.J., Getsios, S., Troyanovsky, S. & Godsel, L.M. Intercellular junction assembly, dynamics, and homeostasis. *Cold Spring Harbor perspectives in biology* **2**, a000125 (2010).

42. Zehendner, C.M., Librizzi, L., de Curtis, M., Kuhlmann, C.R. & Luhmann, H.J. Caspase-3 contributes to ZO-1 and Cl-5 tight-junction disruption in rapid anoxic neurovascular unit damage. *PloS one* **6**, e16760 (2011).
43. Zhou, M. *et al.* Caspase-3 regulates the migration, invasion and metastasis of colon cancer cells. *Int J Cancer* **143**, 921-930 (2018).
44. Huang, Q. *et al.* Caspase 3-mediated stimulation of tumor cell repopulation during cancer radiotherapy. *Nature medicine* **17**, 860-866 (2011).
45. Gramates, L.S. *et al.* FlyBase at 25: looking to the future. *Nucleic acids research* **45**, D663-D671 (2017).

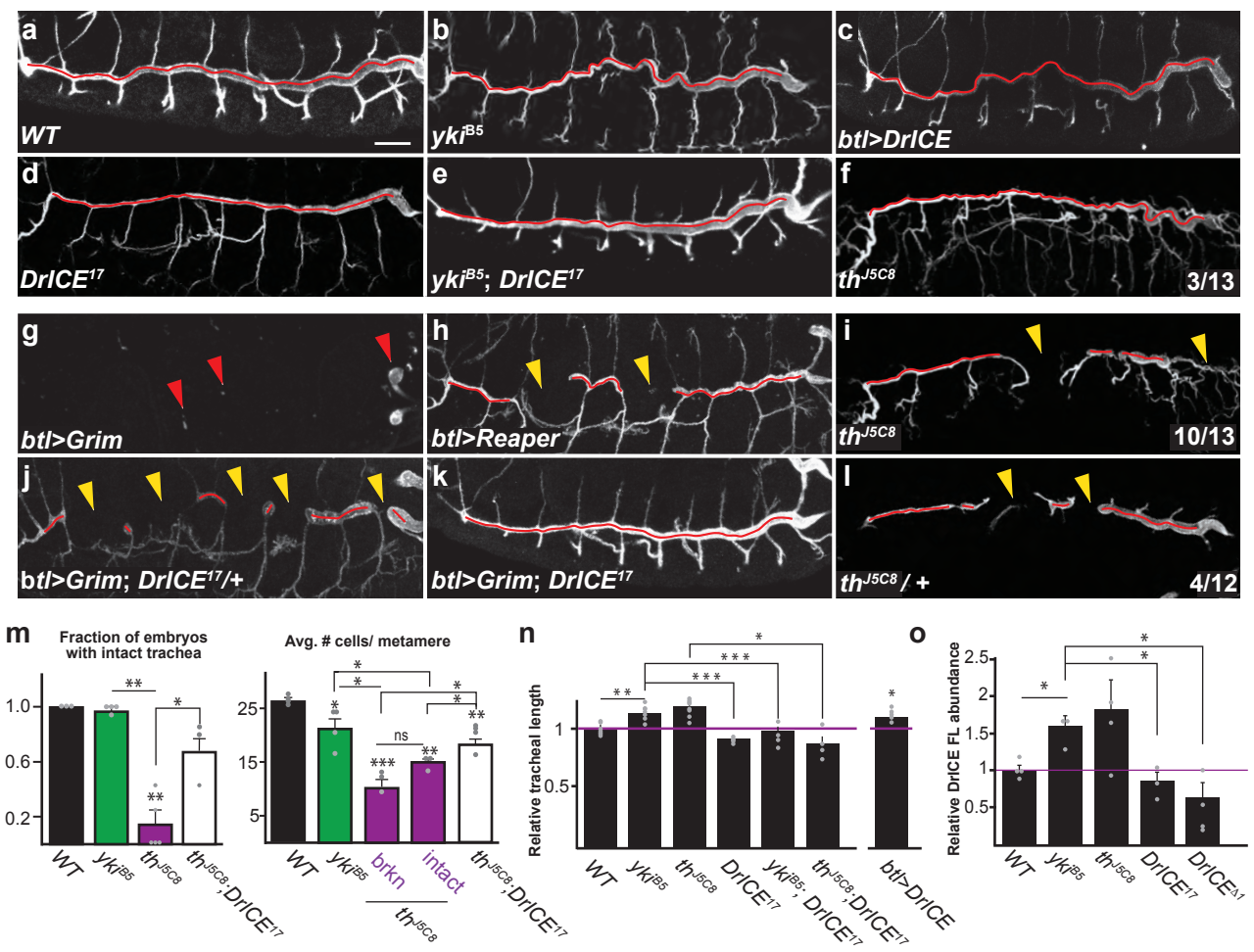
a
WT
b
yki^B5
c
btl>DrICE
d
DrICE^17
e
yki^B5; DrICE^17
f
th^J5C8
3/13
g
btl>Grim
h
btl>Reaper
i
th^J5C8
10/13
j
btl>Grim; DrICE^17/+
k
btl>Grim; DrICE^17
l
th^J5C8 / +
4/12
m
Fraction of embryos with intact trachea
Avg. # cells/ metamere
n
Relative tracheal length
o
Relative DrICE FL abundance
WT
yki^B5
th^J5C8
th^J5C8;DrICE^17
brkn
intact
DrICE^17
yki^B5; DrICE^17
btl>DrICE
DrICE^Δ1
ns

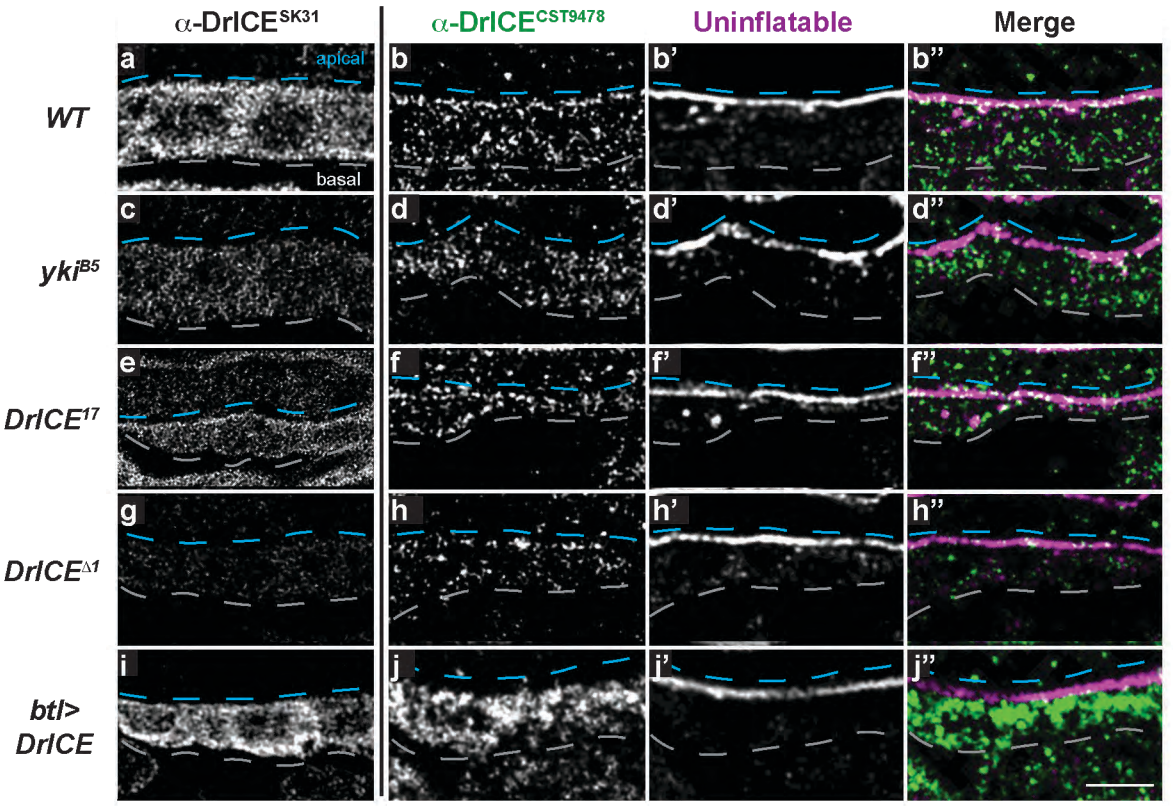
α-DrICE^{SK31}
α-DrICE^{CST9478}
Uninflatable
Merge
WT
yki^{B5}
DrICE^{17}
DrICE$^{\Delta 1}$
btl> DrICE
apical
basal
a
b
b'
b''
c
d
d'
d''
e
f
f'
f''
g
h
h'
h''
i
j
j'
j''

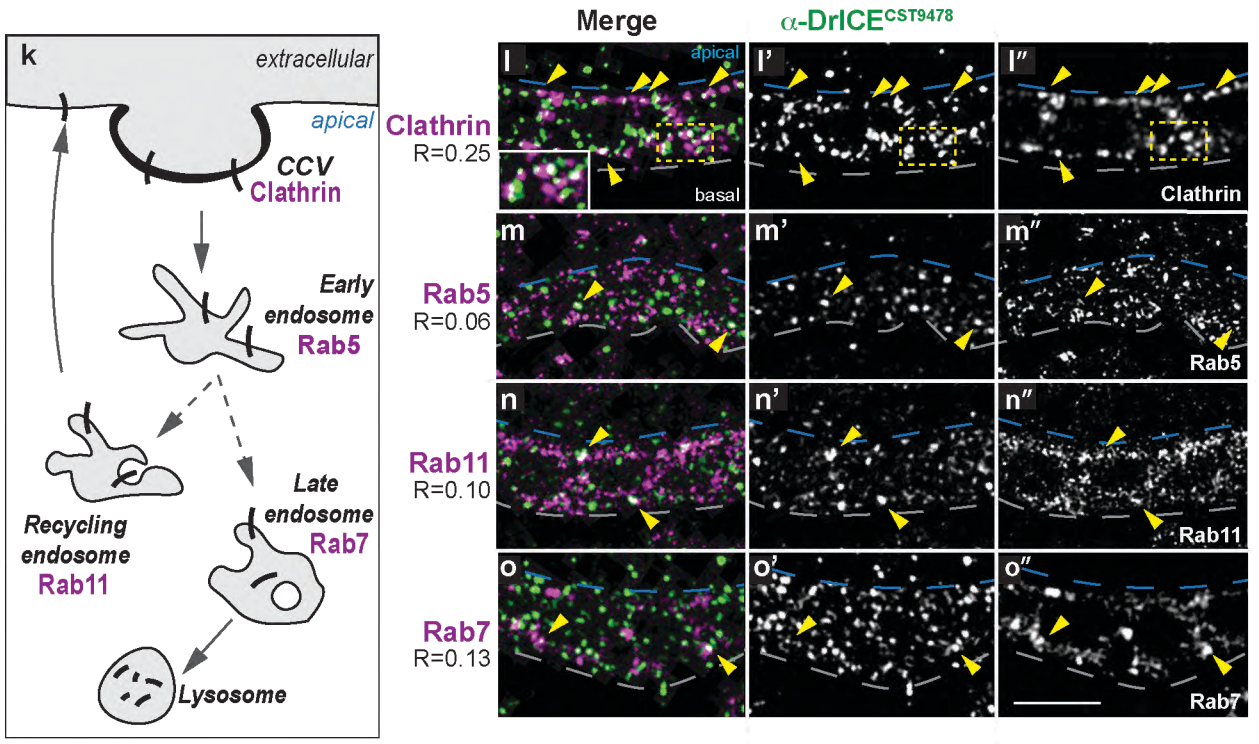
k
extracellular
apical
CCV
Clathrin
Early endosome
Rab5
Recycling endosome
Rab11
Late endosome
Rab7
Lysosome
Merge
α-DrICE^{CST9478}
Clathrin
R=0.25
Rab5
R=0.06
Rab11
R=0.10
Rab7
R=0.13
apical
basal
l
l'
l''
m
m'
m''
n
n'
n''
o
o'
o''

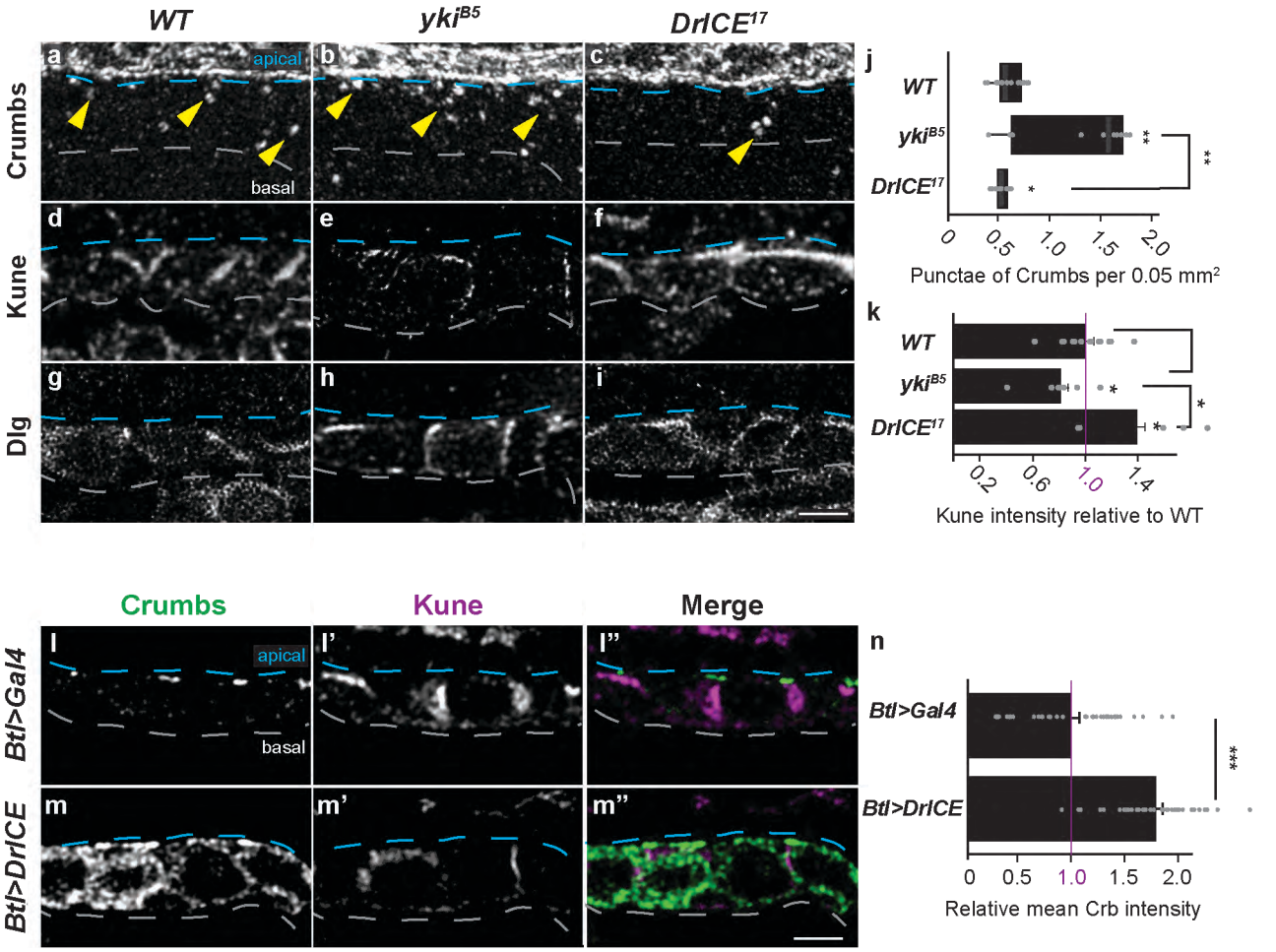
WT
yki^{B5}
DrlCE^{17}
Crumbs
Kune
Dlg
apical
basal
a
b
c
d
e
f
g
h
i
j
WT
yki^{B5}
DrlCE^{17}
0
0.5
1.0
1.5
2.0
Punctae of Crumbs per 0.05 mm^2
k
WT
yki^{B5}
DrlCE^{17}
0.2
0.6
1.0
1.4
Kune intensity relative to WT
Crumbs
Kune
Merge
Btl>Gal4
Btl>DrlCE
l
l'
l''
m
m'
m''
n
Btl>Gal4
Btl>DrlCE
0
0.5
1.0
1.5
2.0
Relative mean Crb intensity

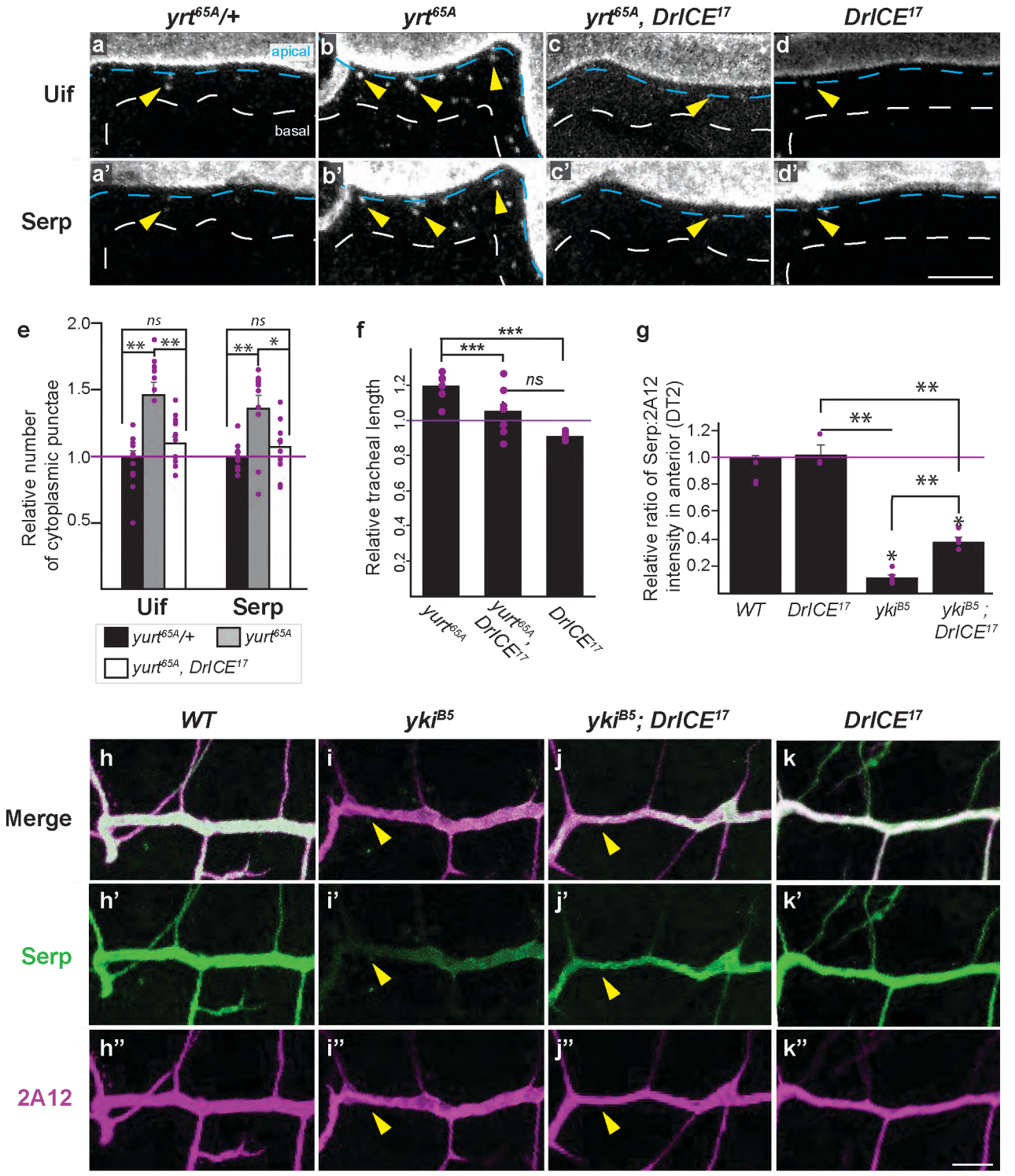
yrt65A/+
yrt65A
yrt65A, DrlCE17
DrlCE17
Uif
Serp
apical
basal
a
b
c
d
a'
b'
c'
d'
e
Relative number of cytoplasmic punctae
2.0
1.5
1.0
0.5
ns
**
*
Uif
Serp
yurt65A/+
yurt65A
yurt65A, DrlCE17
f
Relative tracheal length
***
ns
yurt65A
yurt65A, DrlCE17
DrlCE17
g
Relative ratio of Serp:2A12 intensity in anterior (DT2)
WT
DrlCE17
ykiB5
ykiB5 ; DrlCE17
WT
ykiB5
ykiB5; DrlCE17
DrlCE17
Merge
Serp
2A12
h
i
j
k
h'
i'
j'
k'
h''
i''
j''
k''

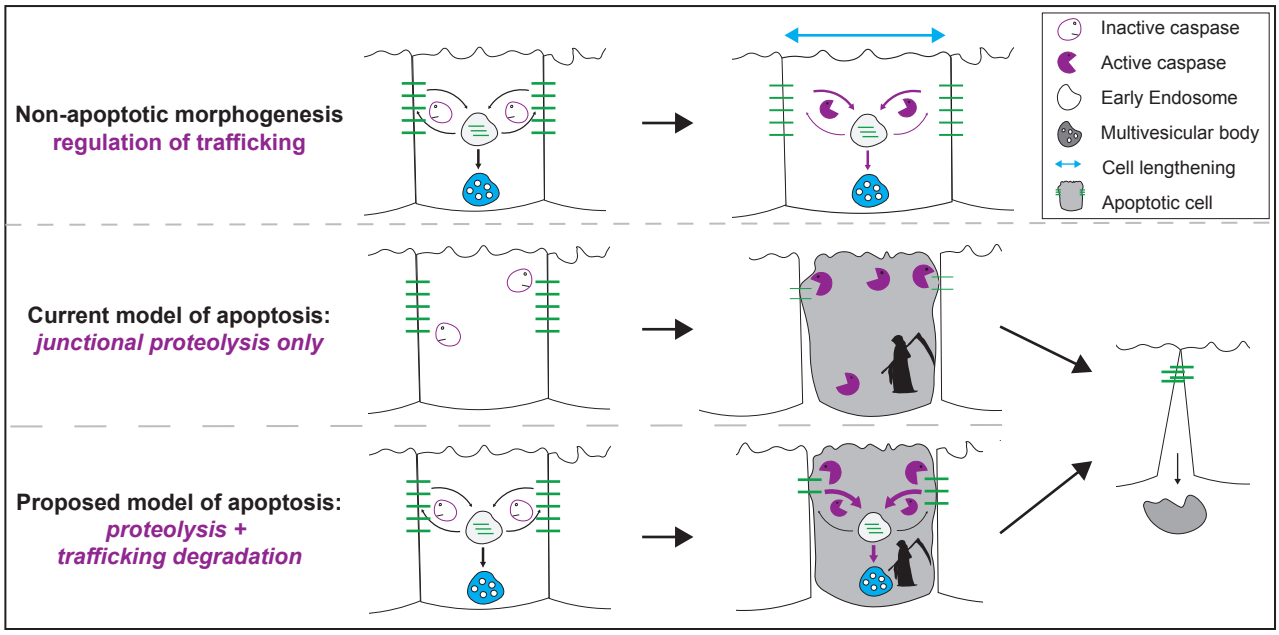
Non-apoptotic morphogenesis
regulation of trafficking
Current model of apoptosis:
junctional proteolysis only
Proposed model of apoptosis:
proteolysis +
trafficking degradation
Inactive caspase
Active caspase
Early Endosome
Multivesicular body
Cell lengthening
Apoptotic cell

Supplementary Figure Legends

Supplementary Fig. 1: Developmental profile of DrICE, DrICE colocalizes with Crumbs, and DrICE levels are elevated in Yorkie mutants.

(a-h") The α-DrICE^{SK31} antibody against full-length DrICE^{1} (a,c,e,g) reveals broad cytoplasmic staining during stages 13-16 (St.13- St. 16). Staining with the α-DrICE^{CST9478} antibody that was raised against a peptide that is cleaved during DrICE activation (Cell Signaling technologies #9478) reveals a more restricted punctate pattern that is enriched at the tracheal apical surface (b,d,f,h) where it overlaps with staining for the apical marker Crumbs (Crb, b', d', f', h'), particularly during stages 13 and 14 (b''-c''). Scale bar for a-h" in h", 5 μm.

(I) Western blot of stage 16 embryos using the α-DrICE^{CST13085} antibody that recognizes full-length DrICE (Cell Signaling Technologies #13085). *yki^{B5}* and *th^{J5C8}* mutations appear to increase DrICE protein levels, but based on quantification of the 47kDa DrICE full-length band relative to total protein from three experiments, only the *yki^{B5}* difference is statistically significant (Fig. 1o). Note that DrICE protein levels in *DrICE^{17}* homozygotes are not different than WT, which is consistent with DrICE^{17} being a dominant negative allele that causes more severe tracheal phenotypes than the DrICE$^{\Delta 1}$ null allele.

Supplementary Fig. 2: Cleaved caspase staining is prominent in Diap1/*th* mutants, and DrICE^{CST9478} staining is absent in larval *DrICE$^{\Delta 1}$*null larval imaginal discs.

(a-c) Maximum projections of anti-cleaved caspase-3 staining, considered a marker of apoptotic cells,[2] shows that trachea of stage 13 *th^{J5C8}* embryos have noticeably more cleaved caspase-3 staining than either (b) *yki^{B5}* or (c) *DrICE^{17}* embryos. As *th^{J5C8}* embryos also have a decreased total number of tracheal cells (Fig. 1m), these data support the conclusion that missing in the dorsal trunk segments in *th^{J5C8}* embryos (Fig. 1i) result from increased tracheal cell apoptosis. Scale bar for a-c in c, 25 μm.

(d-g') Staining WT (*w^{1118}*) late larval wing imaginal discs with DrICE^{CST9478} (low magnification view in e; magnification of the boxed region is shown in f) reveals a pattern of subcellular localization similar to embryonic tracheal cells. (e, g) DrICE^{CST9478} staining is absent in *DrICE$^{\Delta 1}$* mutant wing discs, supporting the conclusion that the DrICE^{CST9478} signal present in *DrICE$^{\Delta 1}$* mutant embryos (Fig. 2h) results from maternal contribution of DrICE. (d'-g') DAPI staining of tissue. Scale bar for d-e' in e', 50 μm; for f-g' in g', 10 μm.

References for Supplemental Figure Legends

1. Ditzel, M. *et al.* Inactivation of effector caspases through nondegradative polyubiquitylation. *Molecular cell* **32**, 540-553 (2008).
2. Baer, M.M. *et al.* The role of apoptosis in shaping the tracheal system in the Drosophila embryo. *Mechanisms of development* **127**, 28-35 (2010).

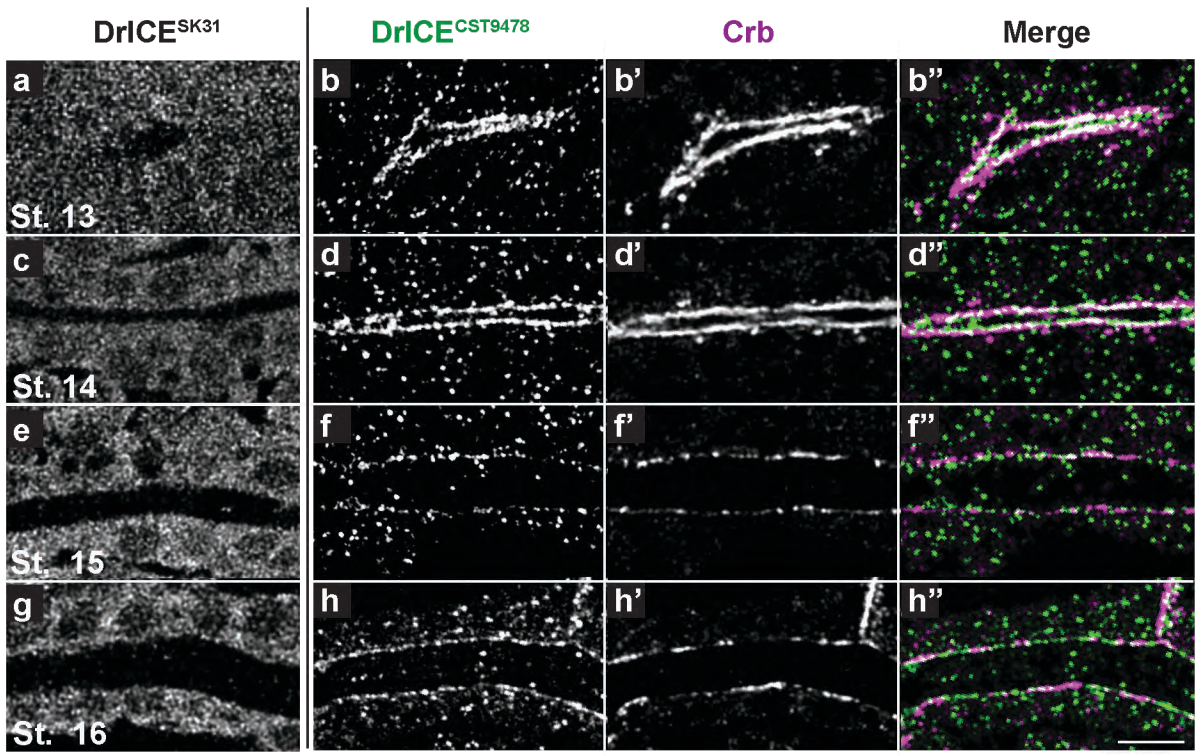
DrICE^{SK31}
DrICE^{CST9478}
Crb
Merge
a
St. 13
b
b'
b''
c
St. 14
d
d'
d''
e
St. 15
f
f'
f''
g
St. 16
h
h'
h''

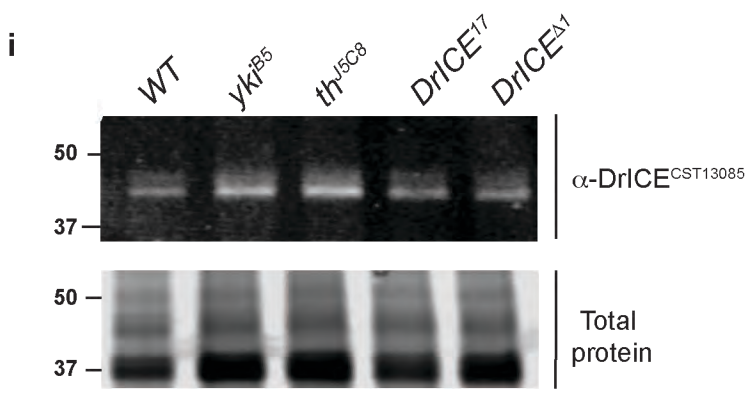
i
WT
ykiB5
thJ5C8
DrICE17
DrICEΔ1
50
37
α-DrICE^{CST13085}
50
37
Total protein

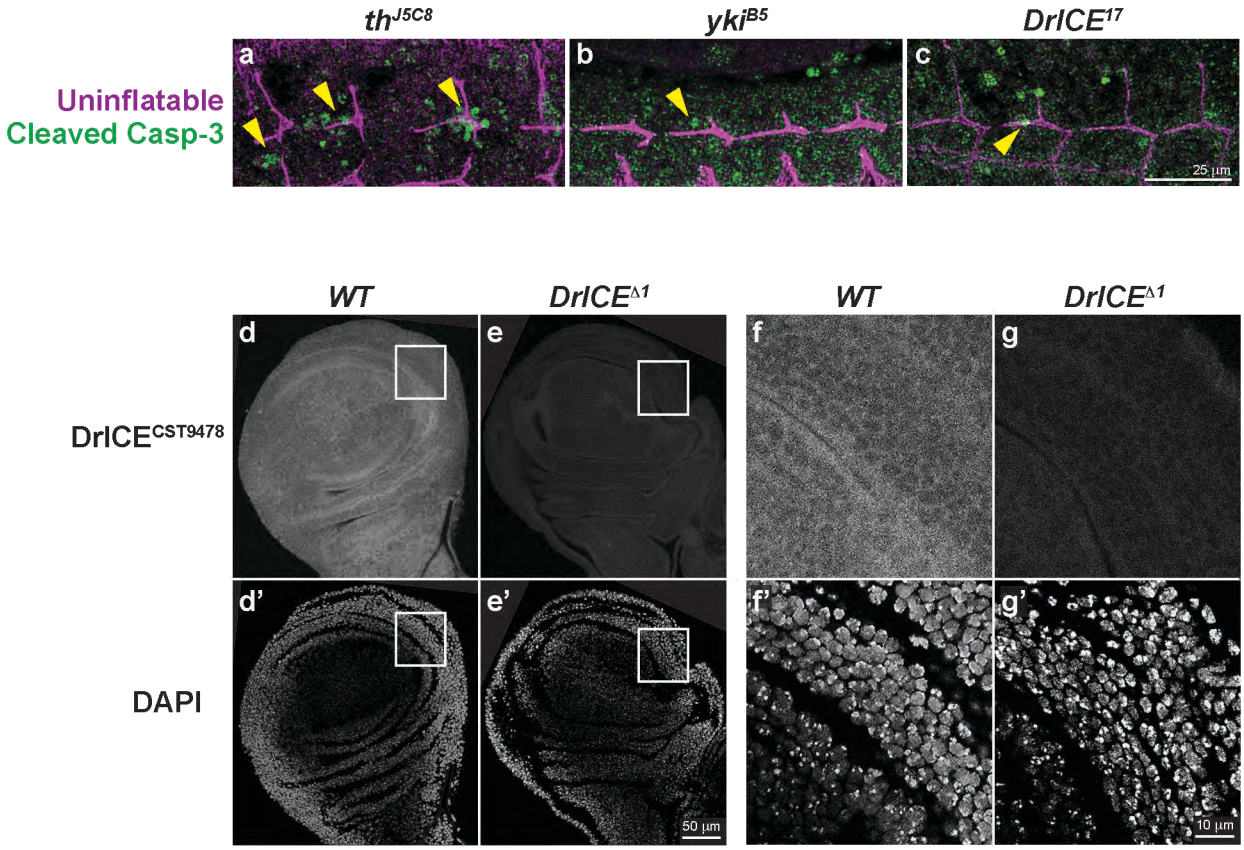
th^J5C8
yki^B5
DrICE^17
Uninflatable
Cleaved Casp-3
a
b
c
25 µm
WT
DrICE^Δ1
WT
DrICE^Δ1
DrICE^CST9478
DAPI
d
e
f
g
d'
e'
f'
g'
50 µm
10 µm

METHODS

Fly Stocks

The following mutant alleles were used in this paper: *th*^{J5C8} [1], *yorkie*^{B5} [2], *DrICE*^{17} [3], *DrICE*$^{\Delta 1}$ [4], *shrub*^{4} [5], and *yurt*^{65A} [6]. DrICE overexpression in the trachea was achieved using the UAS/Gal4 system [7]: the *btl>Gal4* driver was used to express Gal4 in all tracheal cells; *btl>Gal4* flies were crossed to *UAS-DrICE* flies, which had a transgenic DrICE cDNA downstream of UAS (see *Transgenic Constructs* below). The double mutant *yurt*^{65A}*, DrICE*^{17} was generated using standard recombination crosses. Each single male resulting from the recombination crosses was screened for *yurt*^{65A} via failure to a complement *yurt*^{65A} single mutant and screened for the presence of the *DrICE*^{17} mutation by sequencing to identify the point mutation N116Y [3].

Transgenic constructs

To create the UAS-DrICE transgenic line, full length DrICE [3] cDNA sequence was cloned into the MCS of pUAST vector using Gibson cloning and subsequently inserted into the attP2 site into flies with the phiC31 integrase system.

Embryo staining

Parental flies were placed in empty food bottles capped with a molasses-agar plate spread with wet yeast. After 24 hours, plates were removed and embryos were washed with water and fixed using a protocol that largely followed that of Samakovilis et al. (2000). Embryos were dechorionated with 50% bleach for 4 minutes, and fixed in heptane with a 4% formaldehyde solution for 25 minutes. Embryos were then devitellenized for 1 minute with 100% methanol/heptane, rehydrated to PBS-T (0.1% Triton-X100) (100%, 100%, 100%, 50%, each for 5 min), washed in PBST for 5x5' and then 3x30'. PBS-BT (3% BSA in PBS-T) was used to block for 30 minutes at RT before addition of primary antibody, in which embryos were incubated for 48 hours at 4 °C on a rotator. See the attached chart below for appropriate antibody dilutions. PBS-T and PBS-BT steps were repeated on the third day before addition of fluorescent secondary antibodies, in which embryos were incubated O/N at 4 °C. The use of the Alexa+ secondary antibodies (see chart for details) was essential to visualize DrICE α-DrICE^{CST9478} staining as regular Alexa secondary antibodies did not produce adequate signal-to-noise. On the final day, PBS-T washes were repeated, embryos were dehydrated using an ethanol series (50%, 70%, 90%, 100%, 100% EtOH, each for 5 min), incubated in methyl salicylate for 15 min at RT, and then mounted with methyl salicylate and Permount mounting media (Fisher Scientific, SP15-500).

Image acquisition

Confocal z-stacks were obtained with the 63X NA 1.24 oil objective on the Leica SP8 image format greater than or equal to 2048x2048, pinhole size 0.7AU, and system optimized z-step sizes of approximately 0.2 um. Images were subsequently deconvolved using Leica HyVolution software with a Huygens Essential Automatic setting. All quantification was performed on the resulting images.

Image quantification and general statistics

Quantification of junctional components was performed using ImageJ, in which a region of interest in the fifth dorsal trunk metamere of tracheal cells was used to calculate the mean pixel intensity of each junctional component. The number of punctae for Crumbs, Uif, or Serp was calculated by acquiring the number of spots with the ImageJ SpotCounter plugin (Gaussian pre-filtering, box size=8, and noise tolerance=20) and then dividing that number by the total area of that region of interest. Each individual embryo's ratio of spots per unit area was then divided by the WT average, and a Student's 2-tailed t-test was used to calculate the p-value.

Tracheal lengths were determined by Volocity Demo 5.5.1 as previously described [8].

Western blot

Parental flies (heterozygotes with the CyO GMR-dfd YFP or TM6B GMR-dfd YFP balancers[9] were placed in empty food bottles capped with a molasses-agar plate spread with wet yeast. After 1 hour, plates were removed and stored in a humid chamber at 25 °C for 18 hours. Embryos were then washed with water and treated with 50% bleach for 4 minutes. The bleached embryos were sorted to collect only homozygous embryos, which lacked the fluorescent marker denoting the presence of the balancer chromosome. Approximately 30 embryos of each genotype were lysed in RIPA buffer using a micropestle, and then incubated on ice for 30 minutes before 15-minute centrifugation at 4 °C. Protein concentration of the resulting supernatant was measured by Nanodrop 2000 Spectrophotometer (ThermoFisher Scientific), and all samples were diluted with RIPA buffer to the same protein concentration before Laemmeli Buffer was added. Samples were denatured using in a boiling water bath for 5 minutes, loaded in a gradient gel and run for 90 minutes at 100V. Transfer of proteins to the nitrocellulose membrane was carried out at 60V for 20 minutes at 4 °C in order to retain low molecular weight caspases. After total protein levels were detected and imaged using the LiCor REVERT total protein stain and Odyssey CLx imaging system (Li-Cor), blots were incubated in blocking solution (5% BSA in TBS with 0.1% Tween20) for one hour, and then in rabbit anti-*Drosophila* DrICE^{CST13085} (1:1000) overnight at 4°C. Fluorescent Li-Cor goat anti-Rabbit IRDye CW800 secondary antibody was then used to detect the resulting bands, and the mean signal for the 47kd band of each genotype was then normalized to the corresponding lane's total protein signal.

REAGENT or RESOURCE	**SOURCE**	**IDENTIFIER**
Antibodies		
Guinea pig anti-uninflatable (1:800)	Rob Ward	
α-DrICE^{CST9478} Rabbit anti-cleaved Drosophila ICE Asp230 (1:100)	Cell Signaling Technology (CST)	9478S
α-DrICE^{CST13085S} Rabbit anti-Drosophila ICE (1:100)	Cell Signaling Technology (CST)	13085S
Mouse anti-Crumbs extracellular domain (1:25)	Developmental Studies Hybridoma Bank (DSHB) at the University of Iowa	Cq4-s

Mouse anti-2A12 (1:1)		
Rabbit anti-Serp (1:400)		
IRDye 800CW goat anti-Rabbit 0.5mg	Li-Cor	926-32211
Guinea-pig anti-DrICE (SK31)	Pascal Meier	SK31
Rat anti-Clathrin (Chc) (1:40)	Matthias Behr	n/a
Mouse anti-Rab5 (1:100)	BD Biosciences	610281
Mouse anti-Rab7 (1:50)	Developmental Studies Hybridoma Bank (DSHB) at the University of Iowa	Rab7
Mouse anti-Rab11 (1:100)	Fisher Scientific	BDB610656
Guinea pig anti-Melanotransferrin	Christos Samakovilis	n/a
Rabbit anti-Kune-Kune (1:500)	[10]	
Rabbit anti-Dlg (1:500)	Woods et al 1996[11]	
Goat anti-mouse IgG (H+L) highly cross-adsorbed secondary antibody Alexa Fluor 488 Plus	Life Technologies	A32723
Goat anti-mouse IgM (H+L) highly cross-adsorbed secondary antibody Alexa Fluor 488	Life Technologies	A10680
Goat anti-rabbit IgG (H+L) highly cross-adsorbed secondary antibody Alexa Fluor Plus 647	Life Technologies	A32733
Goat anti-guinea pig IgG (H+L) highly cross-adsorbed secondary antibody Alexa Fluor 568	Life Technologies	A11075
IRDye 800CW Goat anti-Rabbit 0.5 mg	Li-Cor	926-32211
Critical Commercial Assays		
REVERT Total protein stain kit	Fisher Scientific	NC1145693
Pre-cast gel 4-15%, 15 well	Bio Rad	4561086
Software and Algorithms		
Fiji (ImageJ) SpotCounter plugin		
Volocity Demo 5.5.1		
Leica Application Suite X (LAS X) HyVolution and colocalization calculation		
Li-Cor Image Studio Software		

References for the Methods

1. Hay, B.A., Wassarman, D.A. & Rubin, G.M. Drosophila homologs of baculovirus inhibitor of apoptosis proteins function to block cell death. *Cell* **83**, 1253-1262 (1995).
2. Silva, E., Tsatskis, Y., Gardano, L., Tapon, N. & McNeill, H. The tumor-suppressor gene fat controls tissue growth upstream of expanded in the hippo signaling pathway. *Current biology : CB* **16**, 2081-2089 (2006).
3. Xu, D. *et al.* The effector caspases drICE and dcp-1 have partially overlapping functions in the apoptotic pathway in Drosophila. *Cell death and differentiation* **13**, 1697-1706 (2006).
4. Muro, I. *et al.* The Drosophila caspase Ice is important for many apoptotic cell deaths and for spermatid individualization, a nonapoptotic process. *Development* **133**, 3305-3315 (2006).
5. Sweeney, N.T., Brenman, J.E., Jan, Y.N. & Gao, F.B. The coiled-coil protein shrub controls neuronal morphogenesis in Drosophila. *Current biology : CB* **16**, 1006-1011 (2006).
6. Laprise, P. *et al.* The FERM protein Yurt is a negative regulatory component of the Crumbs complex that controls epithelial polarity and apical membrane size. *Developmental cell* **11**, 363-374 (2006).
7. Brand, A.H. & Perrimon, N. Targeted gene expression as a means of altering cell fates and generating dominant phenotypes. *Development* **118**, 401-415 (1993).
8. Robbins, R.M., Gbur, S.C. & Beitel, G.J. Non-canonical roles for Yorkie and Drosophila Inhibitor of Apoptosis 1 in epithelial tube size control. *PloS one* **9**, e101609 (2014).
9. Le, T. *et al.* A new family of Drosophila balancer chromosomes with a w- dfd-GMR yellow fluorescent protein marker. *Genetics* **174**, 2255-2257 (2006).
10. Nelson, K.S., Furuse, M. & Beitel, G.J. The Drosophila Claudin Kune-kune is required for septate junction organization and tracheal tube size control. *Genetics* **185**, 831-839 (2010).
11. Woods, D.F., Hough, C., Peel, D., Callaini, G. & Bryant, P.J. Dlg protein is required for junction structure, cell polarity, and proliferation control in Drosophila epithelia. *The Journal of cell biology* **134**, 1469-1482 (1996).